Prediction of Tumor Control in ^{90}Y Radioembolization by Logit Models with PET/CT-Based Dose Metrics

Yuni K. Dewaraja[1], Theresa Devasia[2], Ravi K. Kaza[1], Justin K. Mikell[3], Dawn Owen[3], Peter L. Roberson[3], and Matthew J. Schipper[3]

[1]Department of Radiology, University of Michigan, Ann Arbor, Michigan; [2]Department of Biostatistics, University of Michigan, Ann Arbor, Michigan; and [3]Department of Radiation Oncology, University of Michigan, Ann Arbor, Michigan

The aim of this work was to develop models for tumor control probability (TCP) in radioembolization with ^{90}Y PET/CT–derived radiobiologic dose metrics. **Methods:** Patients with primary liver cancer or liver metastases who underwent radioembolization with glass microspheres were imaged with ^{90}Y PET/CT for voxel-level dosimetry to determine lesion absorbed dose (AD) metrics, biological effective dose (BED) metrics, equivalent uniform dose, and equivalent uniform BED for 28 treatments (89 lesions). The lesion dose–shrinkage correlation was assessed on the basis of RECIST and, when available, modified RECIST (mRECIST) at first follow-up. For a subset with mRECIST, logit regression TCP models were fit via maximum likelihood to relate lesion-level binary response to the dose metrics. As an exploratory analysis, the nontumoral liver dose–toxicity relationship was also evaluated. **Results:** Lesion dose–shrinkage analysis showed that there were no significant differences between model parameters for primary and metastatic subgroups and that correlation coefficients were superior with mRECIST. Therefore, subsequent TCP analysis was performed for the combined group using mRECIST only. The overall lesion-level mRECIST response rate was 57%. The AD and BED metrics yielding 50% TCP were 292 and 441 Gy, respectively. All dose metrics considered for TCP modeling, including mean AD, were significantly associated with the probability of response, with high areas under the curve (0.87–0.90, $P < 0.0001$) and high sensitivity (>0.75) and specificity (>0.83) calculated using a threshold corresponding to 50% TCP. Because nonuniform AD deposition by microspheres cannot be determined by PET at a microscopic scale, radiosensitivity values extracted here by fitting models to clinical response data were substantially lower than reported for in vitro cell cultures or for external-beam radiotherapy clinical studies. There was no correlation between nontumoral liver AD and toxicity measures. **Conclusion:** Despite the heterogeneous patient cohort, logistic regression TCP models showed a strong association between various dose metrics and the probability of response. The performance of mean AD was comparable to that of radiobiologic dose metrics that involve more complex calculations. These results demonstrate the importance of considering TCP in treatment planning for radioembolization.

Key Words: ^{90}Y microspheres; PET/CT; dose–response; radiobiology; radioembolization

J Nucl Med 2020; 61:104–111
DOI: 10.2967/jnumed.119.226472

Radioembolization with ^{90}Y microspheres has gained acceptance as an alternative to chemoembolization for treatment of unresectable hepatocellular carcinoma and liver metastases (*1*). For glass microspheres, the recommended administered activity is calculated to deliver 80–150 Gy to the treated lobe while not exceeding 30 Gy to the lungs (*2*). This calculation, which depends only on the treated liver mass and the lung shunt estimated from pretreatment imaging with ^{99m}Tc-macroaggregated albumin (^{99m}Tc-MAA), assumes a uniform activity distribution in liver without differentiating absorbed doses (ADs) to lesions from those to parenchyma. Although the current approach to radioembolization has led to high rates of tumor response with limited side effects, reported survival is in the range of 8–30 mo (*1,3*). Thus, there is a strong incentive to use dosimetry-guided personalized therapy to achieve more durable responses.

Ultimately, dosimetry-guided treatment planning in radioembolization requires robust relationships between the delivered dose metrics and pretreatment prediction either by the traditional ^{99m}Tc-MAA study or recent (*4*) or future developments. However, dose metrics estimated from posttherapy imaging also have value, potentially as an early predictor of toxicity and response and as a way to plan subsequent radioembolizations (if a multicycle approach were to be used) or subsequent external-beam radiation therapy (EBRT). Furthermore, direct estimates of the delivered dose metrics can be used to establish the dose–outcome models for future predictive imaging-based treatment planning, which is the focus of the current study. Because of the potential for different distributions of the ^{99m}Tc-MAA particles and the microspheres due to various factors, AD estimates from direct ^{90}Y imaging are expected to be more reliable for dose–outcome studies. For glass microspheres, some studies have shown pretreatment ^{99m}Tc-MAA imaging–based AD estimates to be highly predictive of response or survival in hepatocellular carcinoma (*5,6*) whereas others have shown it to be a less reliable surrogate of the microsphere distribution and delivered ADs (*7,8*).

The 2 options for posttherapy imaging in radioembolization, ^{90}Y PET and bremsstrahlung SPECT, are both challenging, but PET is generally considered to have higher quantitative accuracy, especially if Monte Carlo–based scatter correction (*9,10*) is not

Received Jan. 24, 2019; revision accepted May 23, 2019.
For correspondence or reprints contact: Yuni K. Dewaraja, University of Michigan, 1301 Catherine St., 2276 Medical Science I/5610, Ann Arbor, MI 48109.
E-mail: yuni@umich.edu
Published online May 30, 2019.

available for SPECT. For glass microspheres, there have been a few recent reports on dose–response relationships using ^{90}Y PET/CT–derived AD estimates (*11–14*), but only one of these studies considered radiobiology (*14*). The importance of accounting for the biological effects of dose rate and dose nonuniformity using the biological effective dose (BED) and the equivalent uniform dose (EUD) has been demonstrated (*14,15*). The objective of our study was to develop tumor control probability (TCP) models using AD, BED, and EUD metrics derived from an optimized ^{90}Y PET/CT–based 3-dimensional dosimetry protocol. Additionally, we present an exploratory investigation of the association between nontumoral liver AD and liver toxicity.

MATERIALS AND METHODS

Study Population and Treatment

Patients with primary and secondary intrahepatic malignancies scheduled to undergo ^{90}Y radioembolization with glass microspheres (TheraSphere; BTG International Ltd.) at the University of Michigan Medical Center were recruited for ^{90}Y PET/CT imaging and retrospective dosimetry. The study includes all patients treated between January 2015 and March 2018 who met the selection criteria (well-defined lesions > 2 cm^3, ability to undergo imaging, follow-up at the University of Michigan, and informed consent). The patient and lesion characteristics for the 28 lobar treatments (89 lesions) are summarized in Supplemental Table 1 (supplemental materials are available at http://jnm.snmjournals.org). The standard guidelines (*2*) to deliver 80–150 Gy to the treated liver were followed by the treating radiation oncologist, with empiric adjustments within this range based on liver condition, lung shunt, and disease type. The administered activity ranged from 0.5 to 5.8 GBq, and the specific activity of the microspheres at the time of administration ranged from approximately 144 to 1,456 Bq/sphere. The study was approved by the institutional review board, and all subjects signed an informed consent form.

^{90}Y PET/CT Imaging and Quantification

Images were acquired on a Siemens Biograph mCT PET/CT scanner with an acquisition time of about 30 min to cover the entire liver and part of the lung. Time-of-flight PET reconstruction with resolution recovery used 1 iteration, 21 subsets of 3-dimensional ordered-subset expectation maximization, and a 5-mm gaussian postprocessing filter. The PET matrix size was 200×200 with a pixel size of 4.07×4.07 mm and a slice thickness of 3 mm. The CT was performed in low-dose mode (120 kVp; 80 mAs) during free breathing. The CT matrix size was 512×512 with a pixel size of 0.97×0.97 mm and a slice thickness of 2 mm. Since the ^{90}Y PET image was directly available in units of Bq/mL, further calibration factors were not needed for quantification. Volume-dependent recovery coefficients (RCs) were used for mean-value partial-volume correction in volumes of interest because there is currently no well-validated practical method for voxel-level partial-volume correction (*16*).

Phantom Studies to Determine Reconstruction Parameters and RCs

To determine optimal reconstruction parameters under realistic conditions, a ^{90}Y-filled torso phantom with a liver compartment (~1,200 mL) and 3 lesion inserts (29-mL ellipsoid, 16-mL sphere, and 8-mL sphere) was scanned for about 30 min. The insert-to-liver uptake ratio was about 5:1–6:1, and the lung shunt was 5%. The total activity in the phantom was 1.9 GBq, and the activity concentrations were 6.0–7.3 MBq/mL in the inserts and 1.2 MBq/mL in the liver minus the inserts, which are clinically relevant conditions considering previous reports (*6,17*) and the uptake values for the patients in the current study. Both noise (SD divided by the mean in a uniform region of liver background) and activity recovery (PET-estimated activity divided by true activity) were considered when reconstruction parameters were selected. An additional phantom study with 2-, 4-, 8-, 16-, 29-, and 113-mL spheres and a sphere-to-background ratio of 9:1 was performed to generate the RC-versus-volume curve for patient studies. Additionally, we evaluated the quantification accuracy of the liver phantom with and without application of RCs.

Liver and Lesion Segmentation

Liver segmentations performed on diagnostic-quality contrast-enhanced baseline CT or MRI for radioembolization planning were made available to our study, and lesions were manually segmented on these scans by a radiologist specializing in hepatic malignancies. The diagnostic scan was then rigidly registered to the CT portion of the ^{90}Y PET/CT scan, and the contours were transformed with some adjustment of location when misregistration was evident (MIM Software, Cleveland, OH). In some cases in which the lesions were well visualized on the non-contrast low-dose CT portion of the PET/CT scan, they were directly defined on this CT scan to minimize misregistration effects. Up to 5 (largest) lesions were segmented per patient, excluding those smaller than 2 mL, considering the PET spatial resolution and sensitivity to misregistration errors. Nontumoral liver was defined as the total liver volume minus the lesion volumes.

Dosimetric Covariates: AD, BED, EUD, and Equivalent Uniform Biological Effective Dose (EUBED)

Voxel-level dosimetry was performed with our dose-planning-method Monte Carlo code (*18*), with the PET activity map (reconstructed image resampled to match CT size and coregistered) coupled with

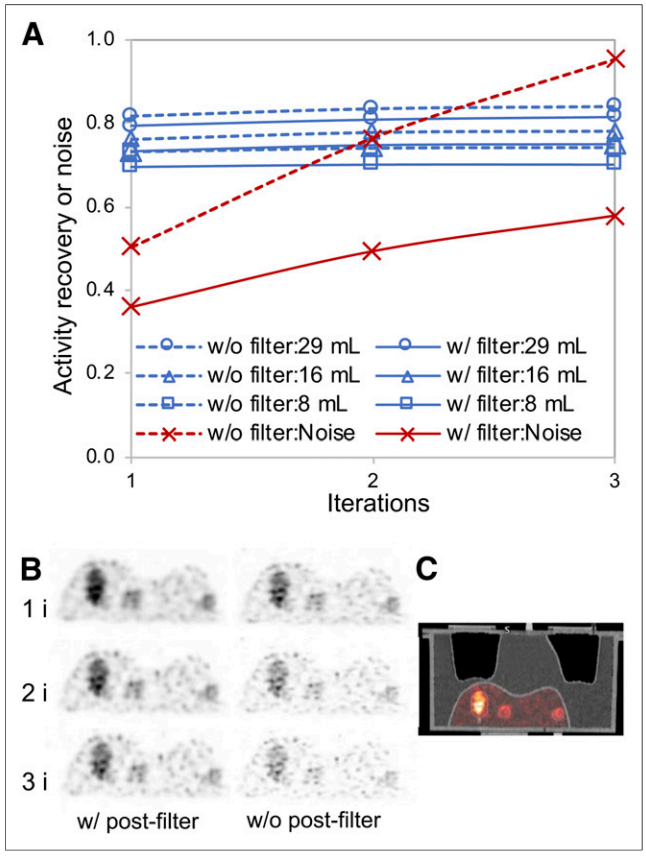

FIGURE 1. ^{90}Y PET/CT liver phantom results. (A) Noise and activity recovery at 1, 2, and 3 iterations (21 subsets) of 3-dimensional ordered-subset expectation maximization with time of flight, resolution recovery, and with and without 5-mm gaussian postprocessing filter. (B) Coronal slice at different iterations. (C) PET/CT corresponding to reconstruction parameters selected for patient study (1 iteration, 21 subsets with filtering).

the CT-derived density map as the input. The dose-rate map was converted to an AD map accounting for physical decay. The voxel-level BED was calculated from differential dose–volume histograms (*19*):

$$\mathrm{BED}_i = D_i + \frac{D_i^2}{\frac{\alpha}{\beta}} \cdot \left(\frac{\lambda}{\lambda + \mu}\right), \qquad \text{Eq. 1}$$

where D_i is the AD at voxel i, λ is the physical decay constant (0.0108/h), μ is the cell repair constant (0.462/h), and α/β (10 Gy) is the ratio of radiosensitivity parameters typical for tumors.

The dose metrics that were considered included lesion mean AD and mean BED (average of voxel-level values) and minimum delivered to a certain percentage xx of the lesion (denoted as ADxx or BEDxx), in increments of 10%. The relative volume that received at least a certain amount of AD or BED (denoted as Vxx) was also determined for the range 50–500 Gy, at intervals of 50 Gy. Additionally, EUD and EUBED were calculated as (*5*)

$$\mathrm{EUD} = -\frac{1}{\alpha} ln\left(\frac{\sum_i e^{-\alpha \cdot D_i}}{N_{\mathrm{vox}}}\right) \qquad \text{Eq. 2}$$

$$\mathrm{EUBED} = -\frac{1}{\alpha} ln\left(\frac{\sum_i e^{-\alpha \cdot \mathrm{BED}_i}}{N_{\mathrm{vox}}}\right), \qquad \text{Eq. 3}$$

where α is the radiosensitivity, the sum is over tumor voxels (i), and N_{vox} is the total number of tumor voxels. We considered a range of α values (0.1–0.0001 Gy^{-1}) to cover the range reported in the literature when estimated from fitting clinical data (*5,14,19–21*).

In addition to the lesion AD metrics, the mean AD to the nontumoral liver was also calculated.

Shrinkage Assessment and Response Classification

Lesion level shrinkage (percentage reduction in largest diameter relative to baseline) on contrast-enhanced CT or MRI using RECIST and modified RECIST (mRECIST) (*22*) at first follow-up was assessed by a radiologist. Lesion response was classified as responding (complete or partial response) or nonresponding (stable or progressive disease). RECIST evaluation was possible for all lesions ($n = 89$), whereas mRECIST evaluation was possible for only a subset ($n = 42$) because arterial-phase images were not available or there was no enhancement in the arterial phase.

Lesion-Level Dose–Response Analysis

Dose–Shrinkage Analysis. First, we investigated the correlation between RECIST or mRECIST lesion shrinkage at first follow-up and mean AD, mean BED, ADxx, BEDxx, and Vxx. This analysis was performed for the 2 subgroups (primary and metastases) and the entire cohort.

TCP Analysis. The TCP models were fit using the various dose metrics as the covariate and using the binary tumor level response classification at first follow-up as the outcome. This analysis was performed for the entire cohort as 1 group and for mRECIST, based on the findings of the dose–shrinkage analysis. The models used a logit link, which is a statistical function commonly applied to relate one or more covariates to the probability of a binary event that has been proposed for EBRT (*23*). Here, a generalized linear mixed-model approach was used with a random intercept term b_k to include patient-level random effects to account for possible correlation between multiple lesions within the same patient. The TCP for the jth lesion for patient k was expressed as

$$\mathrm{TCP}_{jk} = \frac{e^{\beta_0 + b_k + \beta_1 \cdot AD_{jk}}}{1 + e^{\beta_0 + b_k + \beta_1 \cdot AD_{jk}}}, \qquad \text{Eq. 4}$$

with the dose metric under consideration replacing AD. For the EUD covariates, to choose the optimal α, EUD and EUBED for each lesion was first calculated using Equations 2 and 3 for the range of discrete α values. For each α, the maximum-likelihood values of β_0 and β_1 (the slope and intercept of the logistic regression model, respectively) were calculated using standard methods. The α that maximized the likelihood (or equivalently, minimized the $-2\log$[likelihood]) was reported.

Nontumoral Liver AD–Toxicity Analysis

Laboratory liver function test results and ascites classification before treatment and 3 and 6 mo after treatment were used to assess

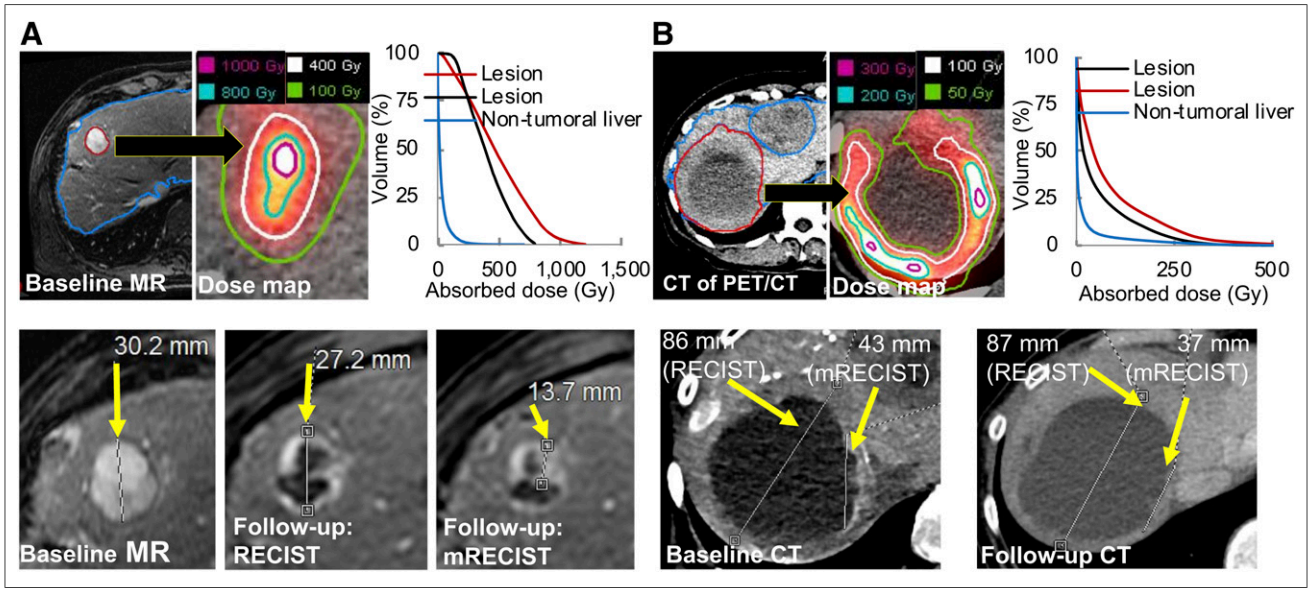

FIGURE 2. Two patient examples showing lesion and nontumoral liver segmentation on baseline MR (A) or CT of PET/CT (B). PET/CT-derived dose maps with isodose contours and dose–volume histograms (top row) and RECIST/mRECIST-based response assessment (bottom row) are also shown. In A, lesion-level classification was stable disease (nonresponding) according to RECIST but partial response (responding) according to mRECIST. In B, classification was stable disease according to both criteria. Not all lesions are shown.

liver toxicity. The correlation between these levels and nontumoral liver mean AD was evaluated. In addition, the association between nontumoral liver AD and ascites classification and Common Terminology Criteria for Adverse Events toxicity classification was also assessed.

Statistical Methods

For lesion dose–shrinkage analysis, linear mixed models were constructed with the dose metrics as the covariate and continuous shrinkage as the outcome. Patient-level random-intercept terms were included to account for possible correlation between multiple lesions within the same patient. Separate models were fit for primary liver cancer versus liver metastases and for shrinkage based on RECIST and mRECIST. Interaction terms were examined for statistically significant differences to determine whether primary and metastatic liver cancer populations could be combined for analysis. The profile likelihood approach (*24*) was used to select the ADxx, BEDxx, and Vxx predictors that gave the best correlation over the range of values considered.

The TCP model parameters were determined by the maximum-likelihood approach that maximizes the probability of predicting the response using Equation 4. TCP model calibration was visually assessed by comparing model-predicted probabilities with observed proportions of response in dose quartiles (dose metrics were considered as continuous variables in the actual analysis; discretization is only for visual representation of the TCP curves). To quantify the predictive power of the TCP models for discriminating among responding versus nonresponding lesions, we calculated the area under the receiver-operating-characteristic curve (AUC). A predicted probability of greater than 50%, which corresponds to a dose threshold of 50% TCP, was used for calculating sensitivity and specificity.

Multiple linear regression models and logistic regression models were used to model the effects of nontumoral liver AD and cirrhosis on the change in liver function tests and on the change in toxicity grade, respectively. All statistical analysis was performed using R, version 3.4.2, and SAS, version 9.4.

RESULTS

Phantom

In the liver phantom study, both increasing the number of iterations and turning off gaussian smoothing increased the noise substantially with only a small gain in activity recovery (Fig. 1). Therefore, 1 iteration (21 subsets) with smoothing (Fig. 1C) was selected for the patient studies. With these parameters, the RCs were 30%, 47%, 60%, 68%, 75%, and 84% going from the smallest to the largest sphere in the multisphere phantom. The activity quantification errors for the liver, 29-mL insert, 16-mL insert, and 8-mL inserts of the liver phantom were 8%, 21%, 27%, and 30%, respectively, without RCs and 1%, 5%, 5%, and 14%, respectively, when volume-dependent RCs were applied. These results generally agree with the quantification accuracy demonstrated in past ^{90}Y PET/CT phantom studies (*25*).

Lesion Uptake and Dosimetry

The lesion and liver segmentation, dose map, and dose–volume histograms are shown in Figure 2 for 2 example cases. Considering all lesions, the median uptake was 5.4 MBq/mL (range, 0.02–28.0 MBq/mL) and the lesion–to–nontumoral treated liver uptake concentration ratio was 4.2 (range, 0.02–39.1). Considering all lesions, the median AD was 268 Gy and the median BED was 404 Gy (summary statistics for all dose metrics are in Supplemental Table 2).

Lesion Shrinkage and Response Rate

Lesion-specific response rates were 27% as assessed by RECIST for all 89 lesions and 57% by mRECIST for the subgroup of 42 lesions that had the required images for mRECIST analysis (RECIST response in this subgroup was 31%). Figure 2 shows examples of response assessment by RECIST and mRECIST.

Lesion-Level Dose–Response Results

Interaction terms of the separate dose–shrinkage models for patients with primary and metastatic lesions revealed no significant differences in any of the examined AD and BED metrics (Fig. 3; Supplemental Tables 3 and 4). Thus, we focused on combined models containing a common intercept and slope for both patient populations.

Increasing AD and BED metrics correlated significantly with increasing tumor level shrinkage as assessed by RECIST or mRECIST for all dose metrics except one (Supplemental Table 2). For all metrics, the correlation was substantially higher for shrinkage based

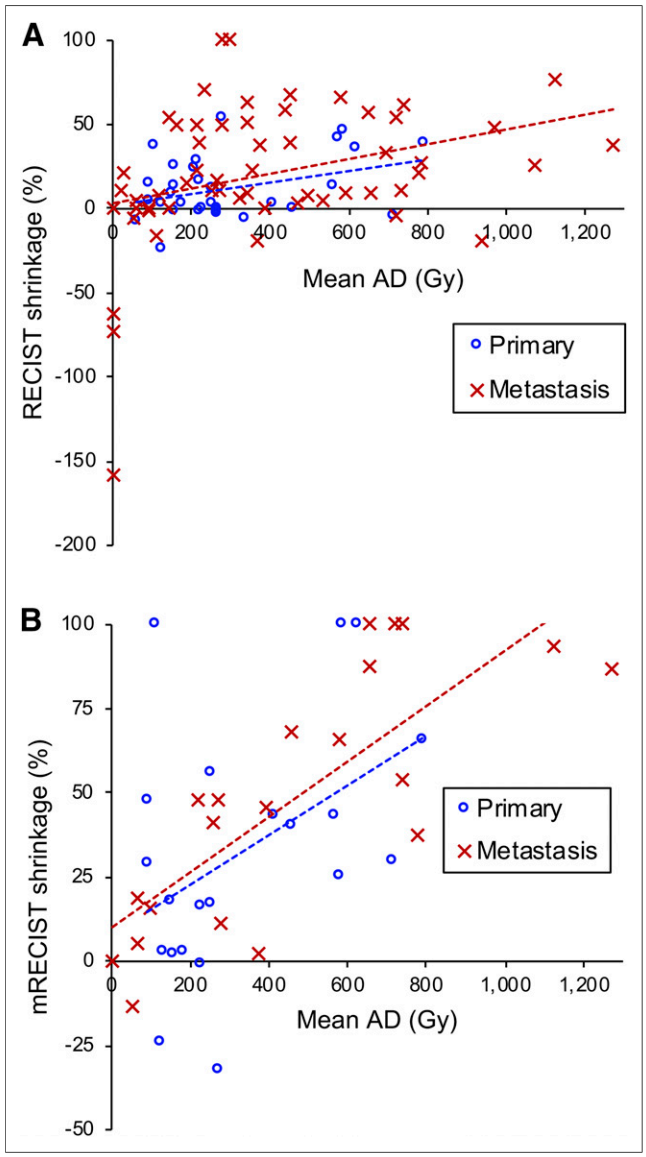

FIGURE 3. Lesion AD–shrinkage relationship separated by lesion type with RECIST assessment (linear mixed model, R^2 = 0.16 for primary, R^2 = 0.05 for metastasis) (A) and mRECIST (linear mixed model, R^2 = 0.19 for primary, R^2 = 0.60 for metastasis) (B). Results for all AD and BED metrics are presented in Supplemental Tables 3 and 4.

on mRECIST than for shrinkage based on RECIST. This is also evident in Figure 3 for AD. Therefore, we focused additional modeling on response as assessed by mRECIST. Furthermore, for liver lesions after radioembolization, the suitability of mRECIST over RECIST is generally accepted (*5,26*).

The ADxx, BEDxx, and Vxx that provided the best shrinkage model fit were AD30, BED50, V500 for AD and V500 for BED. For the various dose metrics, the mean values and ranges for responding versus nonresponding lesions and the associated *P* values are given in Supplemental Table 5.

TCP Model Results

The results from the logit TCP fit are given in Table 1. Univariate logistic regressions with nearly all dose metrics showed significantly increased odds of response with increasing dose. For EUD metrics, results are shown for a range of α values included in the 95% confidence interval for α. Figure 4 shows the model-predicted probability of response as a function of the dose metric plotted alongside observed proportions of response in dose quartiles (quartiles used for visual representation only). The model predictions agree well with the observed proportions for all metrics. Results were similar for the other metrics of Table 1.

Nontumoral Liver AD–Toxicity Results

The median nontumoral liver AD was 38 Gy (range, 8–63 Gy) for patients with cirrhotic livers and 51 Gy (range, 10–83 Gy) for patients with no cirrhosis. Toxicity data were available for 24 of 28 therapies at approximately 3 mo and 22 of 28 at approximately 6 mo. Three patients were excluded from the analysis because their toxicities were not attributable to ^{90}Y. No grade 4 toxicities were observed. New grade 3 toxicity was observed at 3 mo (aspartate aminotransferase [0/21 patients], alanine aminotransferase [0/21 patients], alkaline phosphatase [1/21 patients; cirrhotic liver], and bilirubin [2/21 patients; both cirrhotic]) and at 6 mo (aspartate aminotransferase [0/19 patients], alanine aminotransferase [0/19 patients], alkaline phosphatase [0/19 patients], and bilirubin [2/19 patients; 1 cirrhotic]). Moderate ascites was observed in 3 of 21 (2 cirrhotic) patients at 3 mo and 1 of 19 (cirrhotic) patients at 6 mo. There was no statistically significant correlation between nontumoral liver AD and the liver function test levels, Common Terminology Criteria for Adverse Events classifications, or ascites classification, controlling for cirrhosis.

DISCUSSION

Quantitative ^{90}Y imaging is challenging; hence, we first performed clinically relevant phantom studies to determine reconstruction parameters for our patient studies and to validate the quantification. Whether the liver relative calibration used by some others (*5,26*) or directly using the activity from the PET image, as in the current work, is more accurate needs further investigation. The relative quantification assumes negligible extrahepatic deposition of microspheres and requires accurate measurements of the ^{90}Y vial/residual activity, which can be challenging, but directly using the activity from the PET image can have biases associated with complexities of imaging at the low ^{90}Y PET count-rates (*25*). In the current study, anatomic lesion segmentation was used, because although emission image–based segmentation can be used to identify the tissue with the highest concentration of microsphere deposition, this tissue does not necessarily coincide with the lesion. In a study by Chiesa et al. (*5*), ^{99m}Tc-MAA SPECT thresholding–based segmentation resulted in a 50% TCP of 560 Gy whereas the corresponding value for CT-based segmentation was 390 Gy. The mean AD corresponding to 50% TCP in our study (292 Gy) is

TABLE 1
Results from Logit TCP Models

Dose metric	−2logL	AUC	50% TCP	90% TCP	Sensitivity	Specificity	Dose metric *P*
Mean dose	394.2	0.884	292 Gy	554 Gy	0.750	0.889	0.014
AD30	395.7	0.896	354 Gy	650 Gy	0.792	0.833	0.012
V500 (AD)	388.4	0.872	18%	51%	0.750	0.889	0.109
EUD, $\alpha = 0.0001$ Gy^{-1}	394.2	0.882	291 Gy	552 Gy	0.750	0.889	0.014
EUD, $\alpha = 0.0002^{*}$Gy^{-1}	394.1	0.880	290 Gy	551 Gy	0.750	0.889	0.014
EUD, $\alpha = 0.0005$ Gy^{-1}	394.2	0.877	286 Gy	546 Gy	0.750	0.889	0.014
EUD, $\alpha = 0.002$ Gy^{-1}	395.5	0.873	269 Gy	520 Gy	0.750	0.826	0.014
Mean BED	409.8	0.869	441 Gy	953 Gy	0.760	0.889	0.007
BED50	399.7	0.896	406 Gy	840 Gy	0.750	0.889	0.008
V500 (BED)	389.0	0.866	33.2%	79%	0.875	0.833	0.074
EUBED, $\alpha = 0.0001$ Gy^{-1}	397.8	0.903	463 Gy	890 Gy	0.750	0.889	0.008
EUBED, $\alpha = 0.0005^{*}$Gy^{-1}	396.2	0.903	442 Gy	856 Gy	0.750	0.889	0.009
EUBED, $\alpha = 0.0008$ Gy^{-1}	396.6	0.905	427 Gy	832 Gy	0.750	0.889	0.009
EUBED, $\alpha = 0.002$ Gy^{-1}	398.6	0.884	380 Gy	754 Gy	0.750	0.826	0.009

*Maximum likelihood value of α.

−2logL = log likelihood.

All AUCs were statistically significant, with $P < 0.0001$; 50% and 90% TCP are value of dose metric corresponding to 50% and 90% predicted TCP, respectively. Dose metric *P* is *P* value of dose metric from logistic model. Sensitivity and specificity were calculated using 50% TCP as cutoff for predicted response. Supplemental Table 6 shows results corresponding to full range of α values tested.

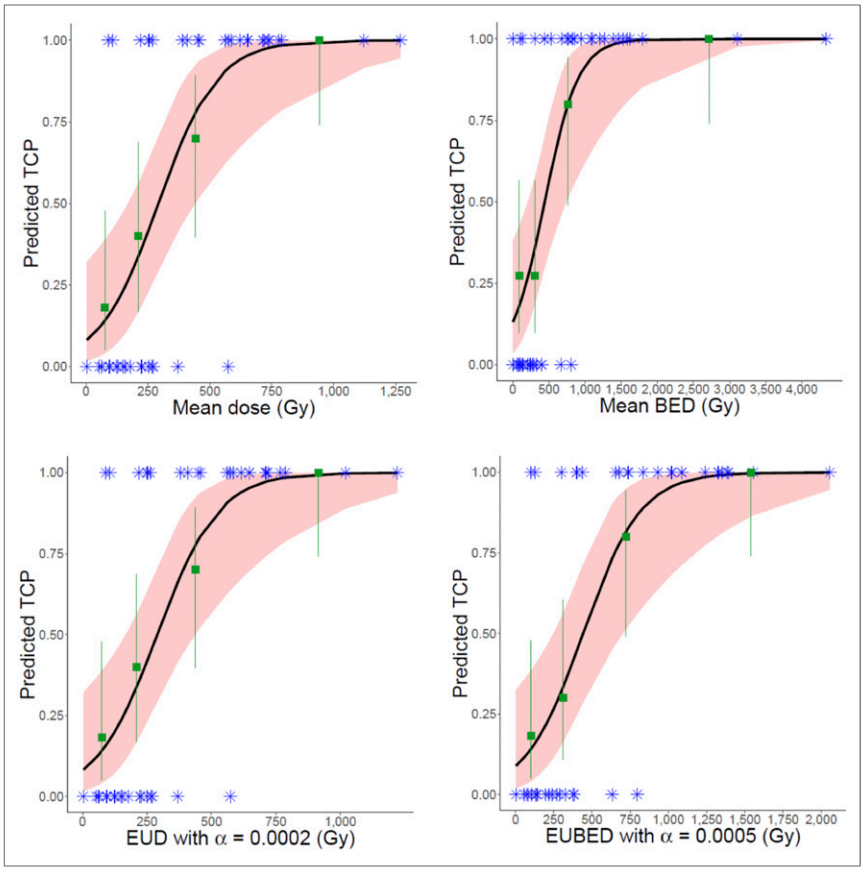

FIGURE 4. Logit model TCP predictions (black curves) compared with observed response proportions (green squares) by dose quartiles. Blue asterisk indicates observed binary response for each lesion. Pink shaded region shows 95% confidence interval for model, and green lines indicate score-based 95% confidence intervals for observations.

between the value reported by Chiesa et al. and the 160 Gy reported by Kappadath et al. (*26*) using bremsstrahlung SPECT/CT–based estimates in hepatocellular carcinoma. The differences in the imaging modalities and activity quantification procedure, as well as in the patient populations, potentially contribute to the observed differences. Because of the importance of considering safety in treatment planning, our dose–toxicity findings for the nontumoral liver in just 24 patients need to be confirmed with a larger cohort. Past studies on hepatocellular carcinoma treated with glass microspheres have reported both the presence (*5*) and the lack (*26*) of a dose–toxicity relationship.

The suitability of the logit function for describing tumor dose–response relationships was evident from the high AUC, sensitivity, and specificity of Table 1 and the good visual agreement of the fits of Figure 4. Although the logit model has no radiobiologic basis, it uses a variable function to approximate the sigmoidal response function potentially caused by tumor variations in radiosensitivity, clonogen number, experimental uncertainty, and other factors. Another TCP model used in EBRT, the radiobiologic Poisson cell survival model (*27*), is based on the assumption that all clonogenic cells need to be eradicated for tumor control. The basic Poisson model allows for the statistical variation in clonogen cell kill (allows for the sigmoidal shape to a limited extent) but does not allow for expected tumor property variability and measurement errors present in clinical data. Thus, this model is not expected to fit the data as well as the logit function. We initially explored other models (Supplemental Fig. 1; Supplemental Table 7) but found that the logit model performed better. For EBRT, more sophisticated models have been proposed (*27,28*) to overcome the limitations of the basic Poisson model, and investigation of such models for radioembolization will be the focus of a future study.

In our study, the macroscopic intralesion AD nonuniformity is included (Fig. 2), but microscopic dose nonuniformity due to nonuniform microsphere deposition is not, as it is well beyond the spatial resolution capabilities of PET. The α value derived from clinical radioembolization data has been described as an "apparent" α (*5*) and is expected to be substantially lower than either the value corresponding to in vitro studies (0.1–0.43 Gy^{-1}) (*29,30*) or the value extracted from clinical EBRT data (0.01 Gy^{-1} for hepatocellular carcinoma) (*21*), for which the dose distribution is uniform. This discrepancy is evident in 2 past studies (*5,19*) and in our results, where the observed α values consistent with a good fit were in the range of 0.0001–0.002 Gy^{-1}. Low apparent radiosensitivity implies high apparent EUD metrics as observed in our study. Furthermore, EUD metrics and TCP model fits will depend on imaging modalities and parameters, which are a focus of an ongoing investigation (*31*). In a recent study, d'Abadie et al. (*14*) used minimal smoothing of PET data to better represent the underlying activity distribution to reconcile differences in observed dose–outcome relationships for resin versus glass microspheres. Another factor that affects the AD distribution is the method used for voxel-level dosimetry. When low-resolution emission images are used as the activity map, whether it is more accurate to assume local energy deposition or to include electron transport (as with Monte Carlo) depends on multiple factors, including resolution, voxel size, and image noise, which is particularly relevant for low-count ^{90}Y PET (*32,33*).

The value of radiobiologic dose metrics over AD for dose–outcome assessment has been demonstrated in limited studies in internal therapy (*14,15*). In our study, although EUBED best discriminated between responding and nonresponding lesions (AUC, 0.90), all the considered dose metrics, including AD, performed well (AUC, >0.87). This result is explained by the nearly linear relationship between AD and the other dose metrics observed for the best fit to our data (Fig. 5). The points that deviate substantially from a linear relationship are mostly at very high values of the dose metrics, where there was good response. Furthermore, at the low α values observed, EUD mathematically approximates AD even for high ADs. If the imaging system has sufficient resolution to resolve microscopic nonuniformities, these results may not hold.

Limitations of the current study include the small sample size, because of which we limited our analysis to lesion-level response instead of patient-level response and analyzed data from only the first follow-up to minimize loss to follow-up. Although, ideally, multiple follow-up points should have been used, studies have

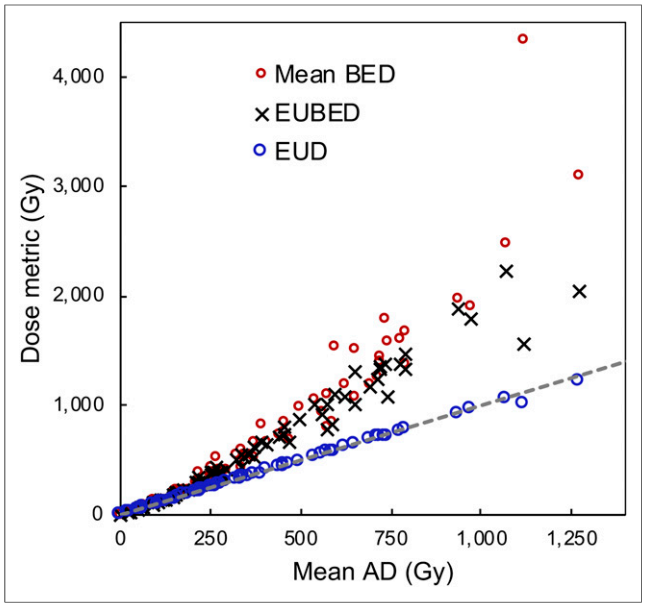

FIGURE 5. Lesion AD vs. BED and EUD metrics. Mean values correspond to average of voxel values within lesion. EUD metrics correspond to optimal α values. Dashed line is identity line.

shown that application of mRECIST as early as 1–3 mo after therapy may be a reliable predictor of outcome and survival after chemoembolization and radioembolization in liver malignancies (*34,35*). A potential confounding factor that was not investigated is the impact of variability in microsphere specific activity (Bq/sphere) at the time of administration. It has been suggested that variability affects the distribution of the spheres at the microscopic level and therefore the efficacy and toxicity (*36*). Another limitation was the heterogeneous patient population. Although we found no significant differences in model parameters between patients with primary lesions and patients with metastatic lesions, this could be because the study was not powered to detect such differences. However, the data did suggest that it was reasonable to fit combined models to all patients, as we did, which allowed more efficient and precise parameter estimates. In addition to analyzing survival data, we will seek—with the accrual of more patients—to further investigate whether separate models are needed for the primary and metastatic groups.

CONCLUSION

In this heterogeneous group of patients, the logit regression TCP model with EUBED showed the best discrimination between responding and nonresponding lesions, but the mean AD, which is relatively simple to estimate in a clinical setting, also performed well, with comparable AUC. These results derived from ^{90}Y PET/CT imaging–based dosimetry should motivate further development of reliable surrogate pretherapy imaging procedures that accurately predict lesion dosimetry for using TCP in treatment planning.

DISCLOSURE

This work was supported by grant R01 EB022075, awarded by the National Institute of Biomedical Imaging and Biomedical Imaging, U.S. Department of Health and Human Services. Yuni Dewaraja is a consultant for MIM Software Inc, Cleveland, Ohio, No other potential conflict of interest relevant to this article was reported.

ACKNOWLEDGMENTS

We thank Stephan Walrand, PhD, for the useful discussions and insightful comments and Chris Maurino and Jeremy Niedbala for data collection and processing.

KEY POINTS

QUESTION: Can lesion dose metrics derived from quantitative posttherapy PET/CT imaging, including metrics that account for radiobiology, be used to accurately predict tumor control in ^{90}Y microsphere radioembolization?

PERTINENT FINDINGS: Logistic regression TCP models were developed to fit clinical dose–response data from patients with liver malignancies treated with ^{90}Y radioembolization. For the subset of 42 lesions with mRECIST response available, all dose metrics that were considered were significantly associated with the probability of response, with AUC greater than 0.87, sensitivity greater than 0.75, and specificity greater than 0.83.

IMPLICATIONS FOR PATIENT CARE: The good association between tumor dose metrics and response demonstrates the importance of considering TCP in treatment planning to improve the efficacy of the treatment in future patients.

REFERENCES

1. Salem R, Gabr A, Riaz A, et al. Institutional decision to adopt Y90 as primary treatment for hepatocellular carcinoma informed by a 1,000-patient 15-year experience. *Hepatology.* 2018;68:1429–1440.
2. TheraSphere Ytrium-90 Glass Microspheres [package insert]. https://www.btg-im.com/BTG/media/TheraSphere-Documents/PDF/TheraSphere-Package-Insert_USA_Rev-14.pdf. Accessed July 23, 2019.
3. Dominello M, Bowers J, Zaki M, Konski A. Radiotherapy and radioembolization for liver metastases. *Ann Palliat Med.* 2014;3:104–113.
4. Prince JF, van den Bosch MAAJ, Nijsen JFW, et al. Efficacy of radioembolization with ^{166}Ho-microspheres in salvage patients with liver metastases: a phase 2 study. *J Nucl Med.* 2018;59:582–588.
5. Chiesa C, Mira M, Maccauro M, et al. Radioembolization of hepatocarcinoma with ^{90}Y glass microspheres: development of an individualized treatment planning strategy based on dosimetry and radiobiology. *Eur J Nucl Med Mol Imaging.* 2015;42:1718–1738.
6. Garin E, Lenoir L, Rolland Y, et al. Dosimetry based on ^{99m}Tc-macroaggregated albumin SPECT/CT accurately predicts tumor response and survival in hepatocellular carcinoma patients treated with ^{90}Y-loaded glass microspheres: preliminary results. *J Nucl Med.* 2012;53:255–263.
7. Haste P, Tann M, Persohn S, et al. Correlation of technetium-99m macroaggregated albumin and yttrium-90 glass microsphere biodistribution in hepatocellular carcinoma: a retrospective review of pretreatment single photon emission CT and post-treatment positron emission tomography/CT. *J Vasc Interv Radiol.* 2017;28:722–730.e1.
8. Mikell JK, Majdalany BS, Owen D, Paradis KC, Dewaraja YK. Assessing spatial concordance between theranostic pairs using phantom and patient specific acceptance criteria: application to ^{99m}Tc-MAA SPECT/^{90}Y-microsphere PET. *Int J Radiat Oncol Biol Phys.* 2019;104:1133–1140.
9. Elschot M, Vermolen BJ, Lam MG, et al. Quantitative comparison of PET and bremsstrahlung SPECT for imaging the in vivo yttrium-90 microsphere distribution after liver radioembolization. *PLoS One.* 2013;8:e55742.
10. Dewaraja YK, Chun SY, Srinivasa RN, et al. Improved quantitative ^{90}Y bremsstrahlung SPECT/CT reconstruction with Monte Carlo scatter modeling. *Med Phys.* 2017;44:6364–6376.
11. Fowler KJ, Maughan NM, Laforest R, et al. PET/MRI of hepatic ^{90}Y microsphere deposition determines individual tumor response. *Cardiovasc Intervent Radiol.* 2016;39:855–864.
12. Srinivas SM, Natarajan N, Kuroiwa J, et al. Determination of radiation absorbed dose to primary liver tumors and normal liver tissue using post-radioembolization ^{90}Y PET. *Front Oncol.* 2014;4:255.
13. Chan KT, Alessio AM, Johnson GE, et al. Prospective trial using internal pair-production positron emission tomography to establish the yttrium-90 radioembolization dose required for response of hepatocellular carcinoma. *Int J Radiat Oncol Biol Phys.* 2018;101:358–365.

14. d'Abadie P, Hesse M, Jamar F, Lhommel R, Walrand S. ^{90}Y TOF-PET based EUD reunifies patient survival prediction in resin and glass microspheres radioembolization of HCC tumours. *Phys Med Biol.* 2018;63:245010.
15. Barone R, Borson-Chazot F, Valkema R, et al. Patient-specific dosimetry in predicting renal toxicity with ^{90}Y-DOTATOC: relevance of kidney volume and dose rate in finding a dose-effect relationship. *J Nucl Med.* 2005;46(suppl 1):99S–106S.
16. Erlandsson K, Buvat I, Pretorius PH, Thomas BA, Hutton BF. A review of partial volume correction techniques for emission tomography and their applications in neurology, cardiology and oncology. *Phys Med Biol.* 2012;57:R119–R159.
17. Campbell JM, Wong CO, Muzik O, Marples B, Joiner M, Burmeister J. Early dose response to yttrium-90 microsphere treatment of metastatic liver cancer by a patient-specific method using single photon emission computed tomography and positron emission tomography. *Int J Radiat Oncol Biol Phys.* 2009;74:313–320.
18. Wilderman SJ, Dewaraja YK. Method for fast CT/SPECT-based 3D Monte Carlo absorbed-dose computations in internal emitter therapy. *IEEE Trans Nucl Sci.* 2007;54:146–151.
19. Strigari L, Sciuto R, Rea S, et al. Efficacy and toxicity related to treatment of hepatocellular carcinoma with ^{90}Y-SIR spheres: radiobiologic considerations. *J Nucl Med.* 2010;51:1377–1385.
20. Klement RJ. Radiobiological parameters of liver and lung metastases derived from tumor control data of 3719 metastases. *Radiother Oncol.* 2017;123:218–226.
21. Tai A, Ericksin B, Khater KA, Li A. Estimate of radiobiologic parameters from clinical data for biologically based treatment planning for liver irradiation. *Int J Radiat Oncol Biol Phys.* 2008;70:900–907.
22. Fournier L, Ammari S, Thiam R, Cuénod CA. Imaging criteria for assessing tumour response: RECIST, mRECIST, Cheson. *Diagn Interv Imaging.* 2014;95:689–703.
23. Källman P, Agren A, Brahme A. Tumour and normal tissue responses to fractionated non-uniform dose delivery. *Int J Radiat Biol.* 1992;62:249–262.
24. Casella G, Berger RL. *Statistical Inference*. Pacific Grove, CA: Duxbury Press; 2002:321, 322.
25. Willowson KP, Tapner M, QUEST Investigator Team, Bailey DL. A multicenter comparison of quantitative ^{90}Y PET/CT for dosimetric purposes after radioembolization with resin microspheres: the QUEST phantom study. *Eur J Nucl Med Mol Imaging.* 2015;42:1202–1222.
26. Kappadath SC, Mikell J, Balagopal A, Baladandayuthapani V, Kaseb A, Mahvash A. Hepatocellular carcinoma tumor dose response after ^{90}Y-radioembolization with glass microspheres using ^{90}Y-SPECT/CT-based voxel dosimetry. *Int J Radiat Oncol Biol Phys.* 2018;102:451–461.
27. Gong J, Dos Santos MM, Finlay C, Hillen T. Are more complicated tumour control probability models better? *Math Med Biol.* 2013;30:1–19.
28. Carlone MC, Warkentin B, Stavrev P, Fallone BG. Fundamental form of a population TCP model in the limit of large heterogeneity. *Med Phys.* 2006;33:1634–1642.
29. Wigg AJ, Palumbo K, Wigg DR. Radiotherapy for hepatocellular carcinoma: systematic review of radiobiology and modeling projections indicate reconsideration of its use. *J Gastroenterol Hepatol.* 2010;25:664–671.
30. Gholami YH, Willowson KP, Forwood NJ, et al. Comparison of radiobiological parameters for ^{90}Y radionuclide therapy (RNT) and external beam radiotherapy(EBRT) in vitro. *EJNMMI Phys.* 2018;5:18.
31. Mikell J, Roberson P, Dewaraja YK. A phantom and patient study of EUD in ^{90}Y radioembolization: difference between ^{90}Y PET/CT-based and true EUD, and sensitivity to reconstruction parameters [abstract]. *J Nucl Med.* 2019;60(suppl):273.
32. Mikell JK, Mahvash A, Siman W, Mourtada F, Kappadath SC. Comparing voxel-based absorbed dosimetry methods in tumors, liver, lung, and at the liver-lung interface for ^{90}Y microsphere selective internal radiation therapy. *EJNMMI Phys.* 2015;2:16.
33. Pasciak AS. A comparison of techniques for ^{90}Y PET/CT image-based dosimetry following radioembolization with resin microspheres. *Front Oncol.* 2014;4:121.
34. Yeo DM, Choi JI, Lee YJ, Park MY, Chun HJ, Lee HG. Comparison of RECIST, mRECIST, and Choi criteria for early response evaluation of hepatocellular carcinoma after transarterial chemoembolization using drug-eluting beads. *J Comput Assist Tomogr.* 2014;38:391–397.
35. Camacho JC, Kokabi N, Xing M, Prajapati HJ, El-Rayes B, Kim HS. Modified response evaluation criteria in solid tumors and European Association for the Study of the Liver criteria using delayed-phase imaging at an early time point predict survival in patients with unresectable intrahepatic cholangiocarcinoma following yttrium-90 radioembolization. *J Vasc Interv Radiol.* 2014;25:256–265.
36. Cremonesi M, Chiesa C, Strigari L, et al. Radioembolization of hepatic lesions from a radiobiology and dosimetric perspective. *Front Oncol.* 2014;4:210.